Numerical Simulations of a Line Plume Impinging on a Ceiling in Cold Fresh Water

Alabodite M. George[a,b], Anthony Kay[a,*]

[a] *Department of Mathematical Sciences, Loughborough University, Loughborough, Leicestershire, LE11 3TU, United Kingdom*
[b] *Department of Mathematics, Niger Delta University, Wilberforce Island, Bayelsa State, Nigeria*

Abstract

Laminar plumes from a line source of warm water at the base of a shallow, homogeneous body of cold water (below the temperature of maximum density) were simulated by a computational model. The plume water undergoes buoyancy reversal as it mixes with the cold ambient. If this occurs before the plume has reached the ceiling of the domain, the plume flaps from side to side. Otherwise, it spreads along the ceiling and then sinks, with a vortex enclosed between the rising plume and the sinking flow. Some of the dense, mixed water from the sinking flow is re-entrained into the rising plume, while the rest flows outwards along the floor. However, with high source temperatures, a sufficient volume of warm water eventually builds up to also form a positively buoyant gravity current along the ceiling.

Keywords: Buoyancy reversal, Impinging plume, Numerical simulation, Gravity current

*Corresponding author

Nomenclature

c_p	specific heat capacity
Fr	Froude number
h	domain height
H	dimensionless domain height
k	thermal conductivity
l	domain width
L_{ad}	dimensionless spreading distance in upper part of domain
L_d	dimensionless spreading distance on ceiling
p	pressure
P	dimensionless pressure
Pr	Prandtl number
Re	Reynolds number
Ri	Richardson number
t	time
T	temperature
u	horizontal velocity component
U	dimensionless horizontal velocity component
v	vertical velocity component
V	dimensionless vertical velocity component
x	horizontal coordinate
X	dimensionless horizontal coordinate
x_{in}	half-width of source
y	vertical coordinate
Y	dimensionless vertical coordinate

Greek letters

α diffusivity of heat

β coefficient in density-temperature relation

μ viscosity

ν diffusivity of momentum

ϕ dimensionless temperature

ρ density

τ dimensionless time

Subscripts

in source

m maximum density

∞ undisturbed ambient

1. Introduction

Buoyancy-driven flows resulting from warm discharges into cold fresh water are of interest because of the possibility of buoyancy reversal due to the nonlinear relation between temperature and density in water. Mixing between the discharged water and the ambient may produce water that is denser than both the warm discharge and the cold ambient water, a process termed "cabbeling" by Foster [1]. For example, cooling water from power stations is typically discharged at a temperature approximately 10°C above that of the receiving water [2, 3]. If this receiving water is a lake below the temperature of maximum density (approximately 4°C in fresh water), mixed water at temperatures close to 4°C may be negatively buoyant and descend to the lake bed rather than spreading at the surface. This was the explanation proposed by Hoglund and Spigarelli [4] for the observation of water at a temperature of 5.7°C at the bed of Lake Michigan in the vicinity of a power station outfall while the natural ambient temperature was 0.5°C.

In the laboratory, Marmoush *et al.* [3] used lock-exchange experiments to simulate the flow resulting from a discharge of warm water into a cold lake. A series of experiments by V.I. Bukreev has involved various configurations

of warm water discharge into a cold ambient. These have included classical lock-exchange [5] and a variety of other arrangements in which warm and cold water are brought into contact across a vertical plane [6, 7]. Such experiments demonstrate clearly the effects of buoyancy reversal and the confinement of the flow by the upper boundary of the receiving water, but do not simulate the near-field of a discharge from an outfall, where the flow would be in the form of a buoyant plume or jet. Further experiments by Bukreev have involved injection of jets of warm water into a cold ambient, both horizontally [8] and vertically upwards [9]. In the latter case, buoyancy reversal occurred before the rising plume interacted with the surface of the receiving water, with the initially rising plume forming a fountain; this case, which is shown schematically in Figure 1, was the subject of a computational simulation by George and Kay [10]. The case where a warm plume in cold water impinges on the upper surface before buoyancy reversal has halted its rise has not yet been addressed either experimentally or computationally. On reaching the surface, the warm water is expected to spread as a positively buoyant gravity current until buoyancy reversal due to mixing causes it to sink to the bed (Figure 2); this behaviour has been seen in experimental studies of gravity currents in cold water [3, 5, 6, 7].

Thus we may contrast the behaviour of free plumes and fountains (where there is no interaction with boundaries) with that of confined flows, where there is impingement on a ceiling or free surface. Parameters which control the behaviour of free plumes and fountains are the Froude number Fr and Reynolds number Re at the source, and the Prandtl number Pr of the fluid; alternatively, the Richardson number, $Ri = Fr^{-2}$, may be used instead of the Froude number. If there is a nonlinear temperature-density relationship, leading to buoyancy reversal, there will be a further control parameter, the dimensionless source temperature $\phi_{\rm in}$ (defined below). Free plumes with buoyancy reversal have some similarity to fountains of negatively buoyant fluid, and recent research on free fountains was reviewed in [10]. The dependence on the control parameters of the maximum height of fountains and the time taken to reach that height has been studied, as well as the continuing unsteady behaviour

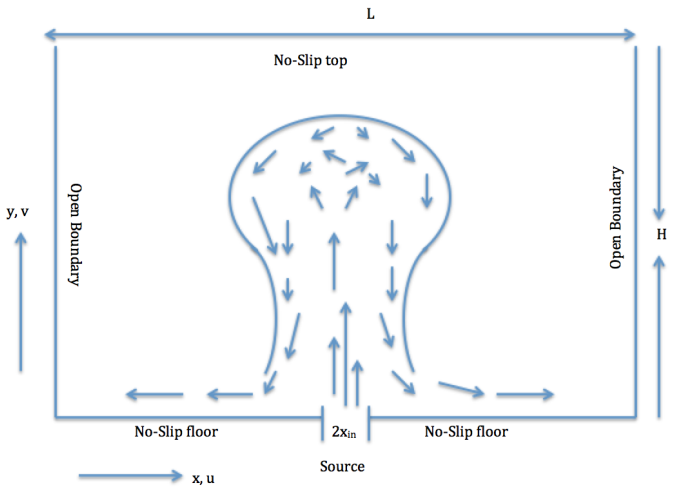

Figure 1: Schematic of plume with buoyancy reversal, also showing domain for computations.

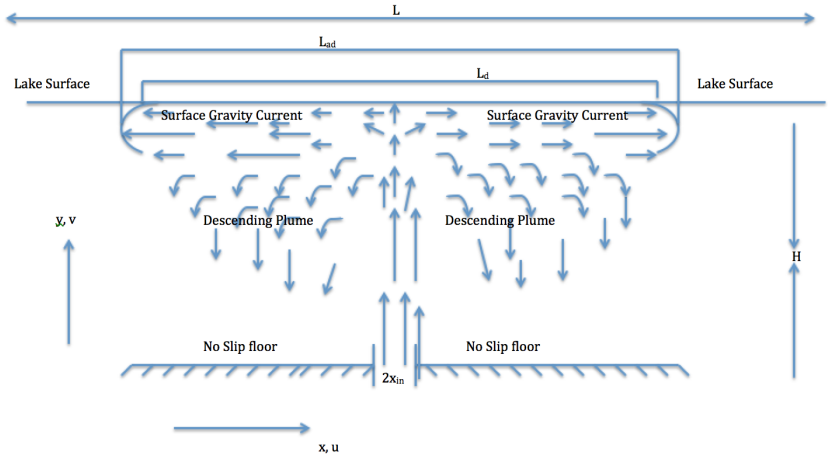

Figure 2: Schematic of plume reaching lake surface before experiencing buoyancy reversal.

("flapping" and "bobbing") which occurs particularly in plumes with buoyancy reversal.

For confined plumes and fountains, the height H of the ceiling or free surface above the source (nondimensionalised with respect to the source half-width or radius) will constitute a further geometrical control parameter. A positively buoyant plume will spread along the upper boundary as a gravity current or "ceiling jet" [11]. However, studies of confined plumes have typically used "filling box" models [12] rather than considering the flow at the surface in detail, although there have been computational studies of natural ventilation flows involving plumes impinging on a ceiling with vents through which buoyant fluid may escape [13, 14]. Confined plumes with buoyancy reversal may initially spread along a ceiling similarly to these positively buoyant flows, but will ultimately behave more like confined fountains, which spread along the upper boundary for some (dimensionless) distance L_d before separating due to negative buoyancy and falling back towards the source level. For such flows, the total distance of travel before separation is $H + L_d$ (also called *augmented spreading distance*), and the dependence of this variable on the control parameters is of interest. Holstein and Lemckert [15] obtained $H + L_d \propto H^{0.5} Fr^{0.4}$ from experiments with fountains impinging on a rigid surface, while Lemckert [16] found $H + L_d \propto Fr^{0.74}$ for fountains impinging on a free surface. Cooper and Hunt [17] made a very detailed experimental study of the flow in an impinging fountain, both in its transient development and its subsequent quasi-steady state: they found that the jet spreading along the surface has thickness increasing linearly with distance from the point of impingement, and that after separation from the surface some fluid is re-entrained into the fountain and surface jet, leading to the formation of a toroidal vortex around the source. Srinarayana *et al.* [18] made a computational study of impinging plane fountains, examining how the behaviour varied with Fr, Re, Pr and H. The fountains were found to settle to a steady state except for $Re \geq 125$ when chaotic behaviour was found, and for $H > 30$ when side-to-side flapping occurred. The augmented spreading distance was found to scale with $Fr^{2/3}$ and with $H^{1/2}$, but to be independent of Re and

Pr. The same authors subsequently modelled the effect of a heat flux at the ceiling, and the resultant stratification, on an impinging plane fountain, and determined the dependence of augmented spreading distance on a dimensionless ceiling temperature as well as Fr and H [19]. A sharp density interface may also provide a form of confinement, and Ansong *et al.* [20] conducted experiments on fountains impinging on such an interface: after overshooting the interface, the flow may return to the floor and/or spread along the interface. However, we are not aware of any previous studies of plumes which experience buoyancy reversal following impingement on an upper boundary or interface.

The purpose of the present article is therefore to report the results of numerical simulations of laminar line plumes that impinge on a rigid, no-slip ceiling, assuming a quadratic dependence of density on temperature as is approximately the case for fresh water below 10°C. The analysis will be carried out for fixed Reynolds and Prandtl numbers, $Re = 50$ and $Pr = 7$, with different dimensionless source temperatures ϕ_{in} and Froude numbers. The ambient is taken to be quiescent and homogeneous, and colder than the temperature of maximum density. The plume is created by injection of warm water, initially less dense than the ambient, at constant speed from a line orifice in the base of the container, so the flow is assumed two-dimensional. Details of the model are given in Section 2, the results of our simulations are presented in Section 3, and we draw some conclusions in Section 4.

2. Model Formulation and Governing Equations

The nonlinear relationship between density ρ and temperature T is fundamental to buoyancy reversal, and the quadratic formula

$$\rho = \rho_m - \beta(T - T_m)^2 \tag{1}$$

with $T_m = 3.98$°C, $\rho_m = 1.000 \times 10^3\,\text{kg.m}^{-3}$ and $\beta = 8.0 \times 10^{-3}\text{kg.m}^{-3}.^\circ\text{C}^{-2}$ gives a good fit to the experimentally determined density of fresh water at temperatures below 10°C [21, 22]. All other fluid properties (e.g. viscosity, thermal

diffusivity) are assumed constant. We assume that the flow is two dimensional, in a rectangular domain of width $l = 40x_{\text{in}}$ and height $h = 10x_{\text{in}}$, where x_{in} is the half-width of the orifice at the centre of the domain floor, through which the warm fluid is injected at mean velocity v_{in}: this computational domain is shown in Figure 1. The velocity profile at the source is assumed parabolic and given as:

$$v(x,0) = \frac{3}{2} v_{\text{in}} \left[1 - \left(\frac{x}{x_{\text{in}}} \right)^2 \right] \tag{2}$$

The inlet temperature T_{in} is assumed constant and the initial ambient temperature T_∞ is uniform.

To define dimensionless variables, the difference between the ambient and the temperature of maximum density provides a natural temperature scale, while the source conditions provide length and velocity scales. Hence, we non-dimensionalise the coordinates x, y, domain dimensions l, h, velocity components u, v, time t, pressure p and temperature T by

$$\begin{aligned} &U = \frac{u}{v_{\text{in}}}\,, \quad V = \frac{v}{v_{\text{in}}}\,, \quad X = \frac{x}{x_{in}}\,, \quad Y = \frac{y}{x_{in}}\,, \quad L = \frac{l}{x_{in}}\,, \quad H = \frac{h}{x_{in}}\,, \\ &\tau = \frac{t}{x_{\text{in}}/v_{\text{in}}}\,, \quad P = \frac{p}{\rho_m v_{\text{in}}^2}\,, \quad \phi = \frac{T - T_\infty}{T_m - T_\infty}, \end{aligned} \tag{3}$$

where x and u are horizontal, y and v are vertical. We take $H = 10$ and $L = 40$ throughout; thus our computational domain is the region $-20 \le X \le 20, 0 \le Y \le 10$. We also define dimensionless parameters, the Reynolds Re, Prandtl Pr and Froude Fr numbers, by

$$Re = \frac{v_{\text{in}} x_{\text{in}}}{\nu}\,, \quad Pr = \frac{\nu}{\alpha}\,, \quad Fr^2 = \frac{\rho_m v_{\text{in}}^2}{g\beta(T_m - T_\infty)^2 x_{in}}, \tag{4}$$

where

$$\nu = \frac{\mu}{\rho}\,, \quad \alpha = \frac{k}{\rho c_p} \tag{5}$$

are the respective diffusivities of momentum and heat, and μ is viscosity, k is thermal conductivity and c_p is specific heat capacity. In terms of these dimensionless variables and parameters, the continuity equation, the horizontal and vertical momentum equations and the thermal energy equation are given as

$$\frac{\partial U}{\partial X} + \frac{\partial V}{\partial Y} = 0 \tag{6}$$

$$\frac{\partial U}{\partial \tau} + U\frac{\partial U}{\partial X} + V\frac{\partial U}{\partial Y} = -\frac{\partial P}{\partial X} + \frac{1}{Re}\left(\frac{\partial^2 U}{\partial X^2} + \frac{\partial^2 U}{\partial Y^2}\right) \tag{7}$$

$$\frac{\partial V}{\partial \tau} + U\frac{\partial V}{\partial X} + V\frac{\partial V}{\partial Y} = -\frac{\partial P}{\partial Y} + \frac{1}{Re}\left(\frac{\partial^2 V}{\partial X^2} + \frac{\partial^2 V}{\partial Y^2}\right) + \frac{1}{Fr^2}\left(\phi^2 - 2\phi\right) \tag{8}$$

$$\frac{\partial \phi}{\partial \tau} + U\frac{\partial \phi}{\partial X} + V\frac{\partial \phi}{\partial Y} = \frac{1}{RePr}\left(\frac{\partial^2 \phi}{\partial X^2} + \frac{\partial^2 \phi}{\partial Y^2}\right) \tag{9}$$

in which the form of the buoyancy term (last term in the vertical momentum equation (8)) is determined by the density formula (1).

The initial conditions for a quiescent ambient are

$$U = 0, \quad V = 0, \quad \phi = 0, \quad \text{for} \quad \tau \leq 0. \tag{10}$$

For $\tau > 0$ we have the following boundary conditions. The sides of the domain are open:

$$\frac{\partial U}{\partial X} = 0, \quad \frac{\partial V}{\partial X} = 0, \quad \frac{\partial \phi}{\partial X} = 0 \quad \text{at} \quad X = \pm\frac{L}{2}\,. \tag{11}$$

The inlet flow has a parabolic velocity profile and a uniform temperature:

$$U = 0, \quad V(X,0) = \frac{3}{2}(1 - X^2), \quad \phi = \phi_{\text{in}} \quad \text{for} \ |X| \leq 1 \quad \text{at} \quad Y = 0, \tag{12}$$

with simulations to be done with two values of dimensionless inlet temperature: $\phi_{\text{in}} = 2.5$ corresponds, for example, to a discharge at 10°C into an ambient at 0°C, while $\phi_{\text{in}} = 4$ would require a discharge at 16°C if the ambient temperature (and hence the Froude number) were the same, but could also represent a discharge at 11.5°C into an ambient at 1.5°C if a 10°C difference was required. The remainder of the floor is a rigid, no-slip, thermally insulated boundary, as is the ceiling:

$$U = 0, \quad V = 0, \quad \frac{\partial \phi}{\partial Y} = 0 \quad \text{for} \quad |X| > 1 \quad \text{at} \quad Y = 0\,, \tag{13}$$

$$U = 0, \quad V = 0, \quad \frac{\partial \phi}{\partial Y} = 0 \quad \text{at} \quad Y = H\,. \tag{14}$$

The source Reynolds number and the fluid's Prandtl number are fixed at $Re = 50$ and $Pr = 7$ in all the computations, while several values of the source Froude number have been investigated as detailed below.

Numerical solution of the above equations is by means of COMSOL Multiphysics software, which uses a finite element solver with discretization by the Galerkin method and stabilisation to prevent spurious oscillations. We have used the "Extra fine" setting for the mesh, which provides the best accuracy consistent with reasonable speed of computation and available memory. Time stepping is by COMSOL's Backward Differentiation Formulas. Further information about the numerical methods is available from the COMSOL Multiphysics website [23].

Results are illustrated below mainly by contour plots of dimensionless temperature on a scale between dark red for the ambient temperature $\phi = 0$, through yellow to white for the source temperature $\phi_{\rm in}$. Note that the same colour represents different temperatures in the two cases, $\phi_{\rm in} = 2.5$ and $\phi_{\rm in} = 4$; but $\phi = 1.0$ always corresponds to the temperature of maximum density while $\phi = 2.0$ is the temperature at which warm water has the same density as the ambient cold water. The contour plots show the entire domain of computation.

3. Results

The evolution of the temperature field for impinging plumes with source Froude number $Fr = 3$ is shown in Figure 3 for dimensionless source temperature $\phi_{\rm in} = 4$ and in Figure 4 for $\phi_{\rm in} = 2.5$. The former case has greater buoyancy, so the initial rise of the plume is faster and it reaches the upper surface earlier; but there is also more rapid mixing in the more buoyant flow, producing a greater volume of dense fluid (near the temperature of maximum density) on its periphery. The presence of this dense mixture causes the plume fluid to start sinking after it has spread a fairly short distance along the ceiling following impingement. A double vortex structure, originally created by the baroclinicity at the edges of the rising plume (Fig. 3 (b)), remains very prominent in this sinking flow. The cores of the vortices are formed of unmixed, warm and positively buoyant fluid, while the sinking flow is maintained by the continual production of dense fluid by mixing. On reaching the floor, dense fluid

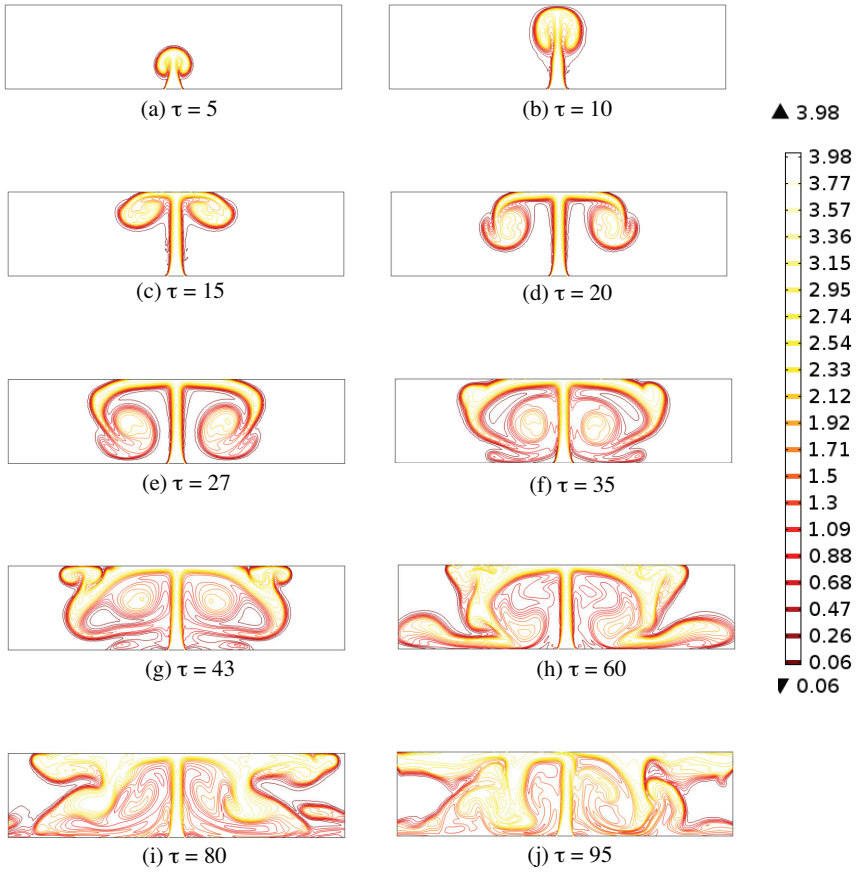

Figure 3: Evolution of temperature field for $Fr = 3$, $\phi_{\text{in}} = 4$ and $Re = 50$ at times $\tau \leq 95$. Colour scale for temperature contours on right.

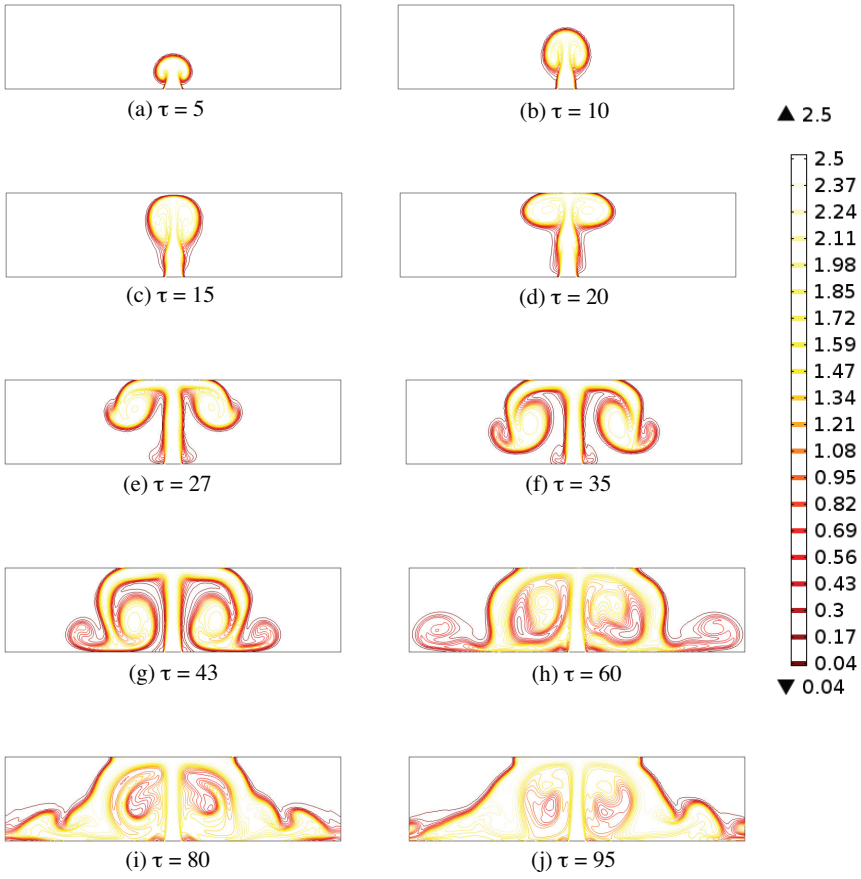

Figure 4: Evolution of temperature field for $Fr = 3$, $\phi_{\text{in}} = 2.5$ and $Re = 50$ at times $\tau \leq 95$. Colour scale for temperature contours on right.

is pulled inwards towards the central rising plume by the vortical motion, and the ambient fluid between the sinking flow and the central plume gets wrapped round the vortex (Figs. 3 (f), 4 (g)). However, as the sinking plume continues to feed dense fluid to the floor, a gravity current begins to form and to move outward (Figs. 3 (h), 4 (g), (h)).

The entire development described so far occurs in both cases illustrated, although it is faster and more vigorous in the case with greater buoyancy; but there is one further feature that is seen only with $\phi_{\text{in}} = 4$. In this case, sufficient positively buoyant fluid reaches the ceiling to form a gravity current along the ceiling. The first sign of this is seen at time $\tau = 35$ (fig. 3 (f)), when there is an upwards bulge in the plume just beyond where it separates from the ceiling. At $\tau = 43$ (Fig. 3 (g)) the ceiling current is starting to develop, but makes little progress; densification by mixing causes this initially buoyant fluid to join the sinking plume (Fig. 3 (h)) at $\tau = 60$, and it is only at $\tau = 80$ (Fig. 3 (i)) that we see the classical profile of a gravity current on the ceiling. However, during the period that the ceiling current is waiting to develop, dense fluid sinks to the floor in sufficient quantities to produce a vigorous gravity current there: this current is barely visible at $\tau = 43$, but has just reached the side of the domain by $\tau = 60$. Subsequently, the ceiling current becomes more vigorous, apparently at the expense of the floor current. We have not continued the simulation beyond $\tau = 95$ because plume fluid has filled much of our domain by this time, but we would expect the ceiling current to eventually be halted as its fluid becomes denser through mixing, and the floor current might then become stronger again.

In contrast, the flow with $\phi_{\text{in}} = 2.5$ becomes more settled at late times. Only a small degree of mixing is required to make the plume water denser than the ambient so, while the mixing is less vigorous than in the more buoyant case, there is never sufficient unmixed warm water at the ceiling to form a gravity current there. So once the sinking flow has formed, the warm water makes no further progress along the ceiling (Fig. 4 (f) – (j)). A dense gravity current moves outward along the floor (Fig. 4 (g), (h)), and behind it a broadening region of sinking, mixed fluid develops (Fig. 4 (i), (j)). The development in the

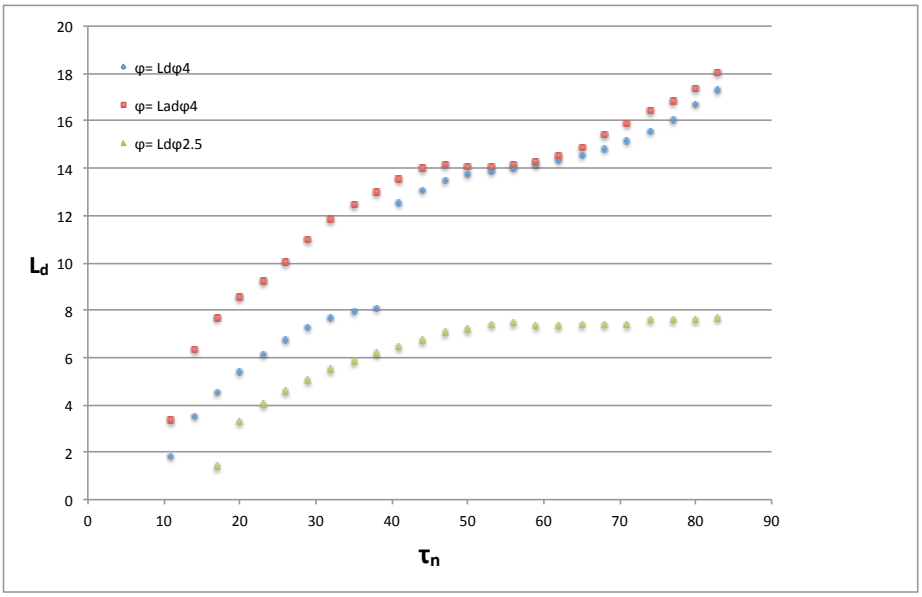

Figure 5: Variation of spreading distance L_d & L_{ad} for $\phi = 2.5$ and 4 with respect to time τ at $Fr = 3$.

case with $\phi_{\text{in}} = 2.5$ is rather similar to that of a negatively buoyant impinging fountain as simulated by Srinarayana *et al.* [18], which has the same double-vortex structure, with re-entrainment of dense fluid from the periphery of the vortices into the central plume, a dense gravity current spreading outwards along the floor, and the flow eventually reaching a steady state.

The contrast between the two cases is further illustrated in Figure 5, which shows the spreading distance L_d of the plume fluid on the ceiling as a function of time. With $\phi_{\text{in}} = 2.5$ (green dots), L_d initially increases rapidly after the warm water reaches the ceiling. The rate of spreading then decreases until $\tau \approx 55$, but beyond this time there is no further increase in L_d, which remains constant at around 7.5. For $\phi_{\text{in}} = 4$ we provide two plots: the blue dots represent L_d, the spread of plume fluid at the ceiling, while the red dots show L_{ad}, its furthest horizontal extent anywhere in the upper part of the domain. The difference between L_d and L_{ad} in the initial rapid spreading phase is due to the curvature of the vortical region and of the subsequent sinking flow, but of more interest

is the behaviour after $\tau = 35$. The sudden jump in L_d at $\tau \approx 40$ is due to the incipient gravity current of positively buoyant fluid (Fig. 3 (g)), and the subsequent constancy of L_{ad} from $\tau \approx 45$ to $\tau \approx 60$ is due to the failure of this current to develop until sufficient further buoyant fluid has accumulated at the ceiling. Following this "waiting period", the gravity current accelerates along the ceiling, with its nose (represented by L_{ad}) somewhat ahead of the flow at the ceiling.

In our earlier work [10] we found that the maximum rise height of plumes increases with Froude number because plumes with low Fr experience more vigorous mixing. Thus plumes will only impinge on a ceiling with sufficient momentum to start spreading sideways if the source Froude number is above some minimum value; for the ceiling height in our domain, we have therefore only considered plumes with $Fr \geq 1.5$. Figure 6 shows the temperature field at time $\tau = 80$ with four different source Froude numbers and with both values of source temperature, $\phi_{\text{in}} = 4$ and $\phi_{\text{in}} = 2.5$. At $Fr = 4$ and $Fr = 5$ the flow is similar to that seen in Figs. 3 (i) and 4 (i): with $\phi_{\text{in}} = 4$ there are vigorous gravity currents at both the floor and ceiling, but with $\phi_{\text{in}} = 2.5$ there is a sloping, descending flow beyond the vortices on either side of the central rising plume. At $Fr = 2.5$ the gravity currents with $\phi_{\text{in}} = 4$ are weaker, while with $\phi_{\text{in}} = 2.5$ the descending flow slopes more steeply and then forms gravity currents along the floor. There is some asymmetry at $Fr = 2.5$, and more so at $Fr = 1.5$; at this lowest Froude number, no ceiling current forms even with $\phi_{\text{in}} = 4$ because the plume loses too much buoyancy as a result of mixing by the time it impinges on the ceiling. However, the dense fluid reaching the floor does produce rather weak gravity currents there.

We have not attempted to determine scalings for augmented spreading distance $H + L_d$ as a function of Fr as was done for negatively buoyant fountains by Srinarayana *et al.* [18]. This might be possible in the case $\phi_{\text{in}} = 2.5$ with further simulations over a wider range of Froude numbers (above about 2), since the flow appears to settle to a steady state within our simulation time; but with $\phi_{\text{in}} = 4$ we would need to determine the ultimate fate of the ceiling gravity cur-

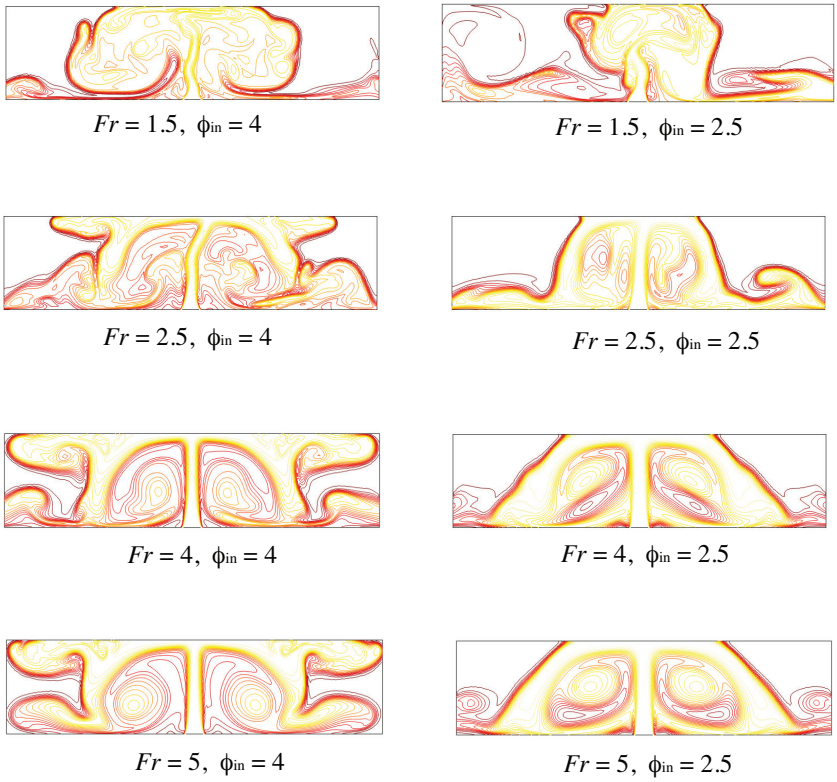

Figure 6: Temperature field at time $\tau = 80$ for various source conditions (Froude number and inlet temperature). Left column: $\phi_{\text{in}} = 4$, for which the colour scale in Fig. 3 applies. Right column: $\phi_{\text{in}} = 2.5$, for which the colour scale in Fig. 4 applies.

rents, which would require a much wider computational domain and a longer time. It is expected that they would eventually be arrested as a result of further densification by mixing [3]. Although we have not been able to continue our computations to verify this, it is still of interest to examine further the earlier development of the ceiling currents by plotting horizontal profiles of temperature and velocity components near the ceiling. Figures 7 – 9 show these profiles at $Y = 9$ (a distance $x_{\rm in}$ below the ceiling) at various times for four different source conditions. With $Fr = 3$ and $\phi_{\rm in} = 4$, Figure 7 (a) shows the somewhat irregular progress of the warm water along the ceiling. The dip in temperature around $2 \leq X \leq 5$ at times $\tau \geq 20$ is due to ambient fluid enclosed within the vortex, and this vortex is also seen as peaks in the outward and downward velocity components around $5 \leq X \leq 7$ in Figures 8 (a) and 9 (a). A well developed gravity current is only apparent at the last time, $\tau = 80$ in Figure 8 (a), although the large temperature fluctuations behind the front at $\tau = 35$ and $\tau = 50$ in Figure 7 (a) indicate the detachment of volumes of warm, buoyant water from the vortex towards the ceiling, where they will subsequently initiate the current. These features are absent in the case with $Fr = 3$ and $\phi_{\rm in} = 2.5$ (Figure 7 (b)), which shows the warm water front almost stalling after $\tau = 35$; in fact it retreats a little between $\tau = 50$ and $\tau = 80$. The vortex is still prominent in this case, with strong outward and downward flow near $X = 5$, and the negative horizontal velocities beyond $X = 9$ at later times (Figure 8 (b)) indicate entrainment of ambient water into the sinking flow (also seen at $\tau = 50$ in Figure 8 (a)). Lower Froude numbers are associated with greater mixing in the central rising plume and Figures 7 (c), (d) show temperatures near the ceiling with $Fr = 1.5$ being lower than in the corresponding cases with $Fr = 3$. Even with $\phi_{\rm in} = 4$ the warm water makes slow progress along the ceiling: the front is competely stalled between $\tau = 20$ and $\tau = 50$, and while it has moved a little further by $\tau = 80$, there is no clear evidence of a gravity current developing (see also Figure 6 (a)). Nevertheless, the vortex is still a prominent feature in the velocity plots, Figures 8 (c) and 9 (c). Finally, with $Fr = 1.5$ and $\phi_{\rm in} = 2.5$, we see large variations in both the temperature and velocity profiles from one

time of plotting to the next. This indicates side-to-side flapping motion: strong mixing of water which is only slightly buoyant at the source means that it has lost all its buoyancy when it impinges on the ceiling, and it behaves similarly to an unconfined plume [10].

The development of the flow at the floor is illustrated best by horizontal profiles of horizontal velocity at height $Y = 1$, shown in Figure 10 (in which the earliest time shown is $\tau = 43$ because the plume fluid has not recirculated to the floor until close to this time). The general appearance of the profiles is rather similar in all cases, with flow inward towards the central plume reaching its greatest speed near $X = 5$, and an outward flow beyond $X = 10$. The flow is stronger with $Fr = 1.5$ than with $Fr = 3$, because the greater mixing with lower Froude number produces dense water more rapidly, yielding a greater volume for both the inward and outward flows. There is also a slight tendency for the inward flow to be stronger with $\phi_{\rm in} = 4$ while the outward flow is stronger with $\phi_{\rm in} = 2.5$; the vortex circulation which brings fluid inward near the floor may be stronger in the former case due to the greater buoyancy in the central plume generating greater vorticity.

4. Conclusions

We have previously simulated plumes with reversing buoyancy in effectively unconfined domains, and noted their similarities with, and differences from, fountains which have negative buoyancy from their source [10]. For impinging plumes which are the subject of the present study, the most directly comparable study of negatively buoyant fountains is that by Srinarayana *et al.* [18]. Within the range of control parameters that we have used, three classes of flow have been found, of which two were also observed in [18].

For sufficiently large Froude number and with $\phi_{\rm in} = 2.5$, the plume develops a double vortex structure. After the plume impinges on the ceiling, the vortices expand to fill the full height of the domain. The flow then appears to approach a steady state (although our computational time was not sufficient to verify this),

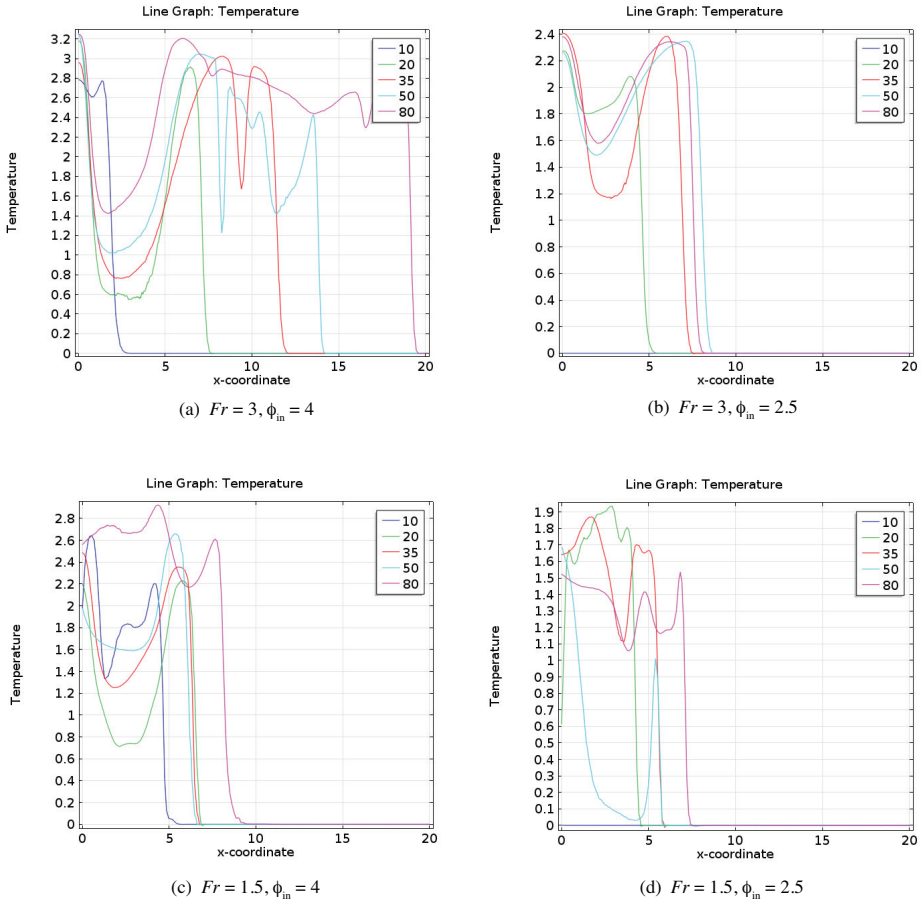

(a) $Fr = 3, \phi_{in} = 4$ (b) $Fr = 3, \phi_{in} = 2.5$

(c) $Fr = 1.5, \phi_{in} = 4$ (d) $Fr = 1.5, \phi_{in} = 2.5$

Figure 7: Horizontal profiles of dimensionless temperature ϕ at $Y = 9$ (near the ceiling), at times $\tau = 10, 20, 35, 50, 80$, for plumes with $Re = 50$, $Pr = 7$, and with Froude number and inlet temperature as indicated below each panel.

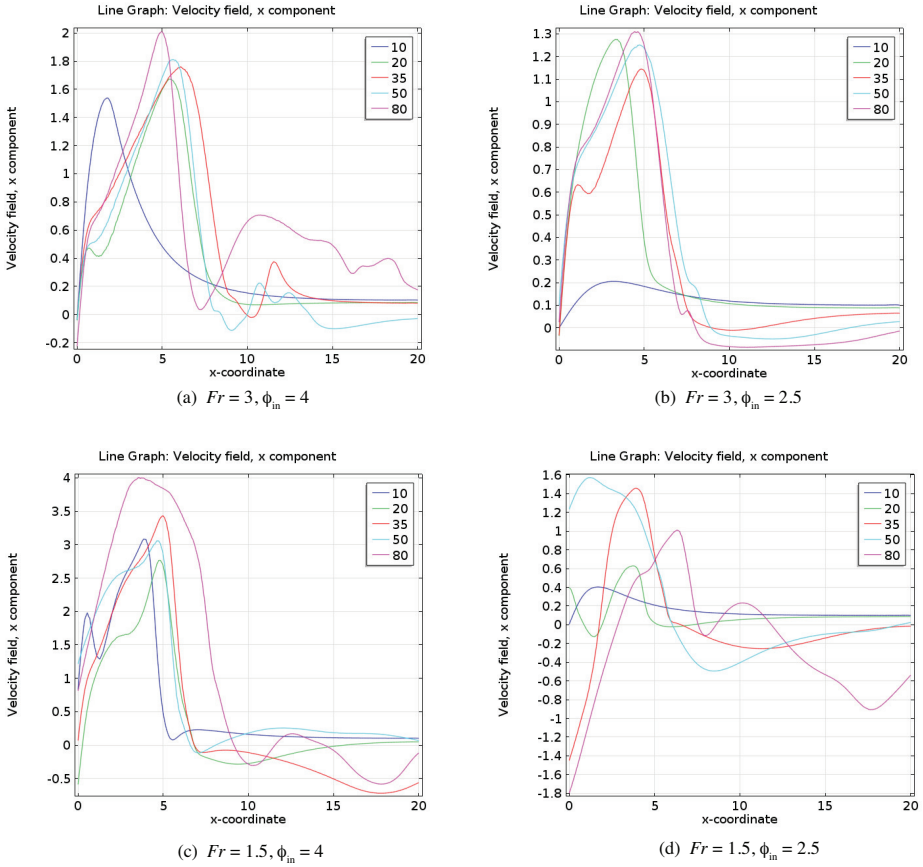

(a) $Fr = 3, \phi_{in} = 4$ (b) $Fr = 3, \phi_{in} = 2.5$

(c) $Fr = 1.5, \phi_{in} = 4$ (d) $Fr = 1.5, \phi_{in} = 2.5$

Figure 8: Horizontal profiles of horizontal velocity component U at $Y = 9$ (near the ceiling), at times $\tau = 10, 20, 35, 50, 80$, for plumes with $Re = 50$, $Pr = 7$, and with Froude number and inlet temperature as indicated below each panel.

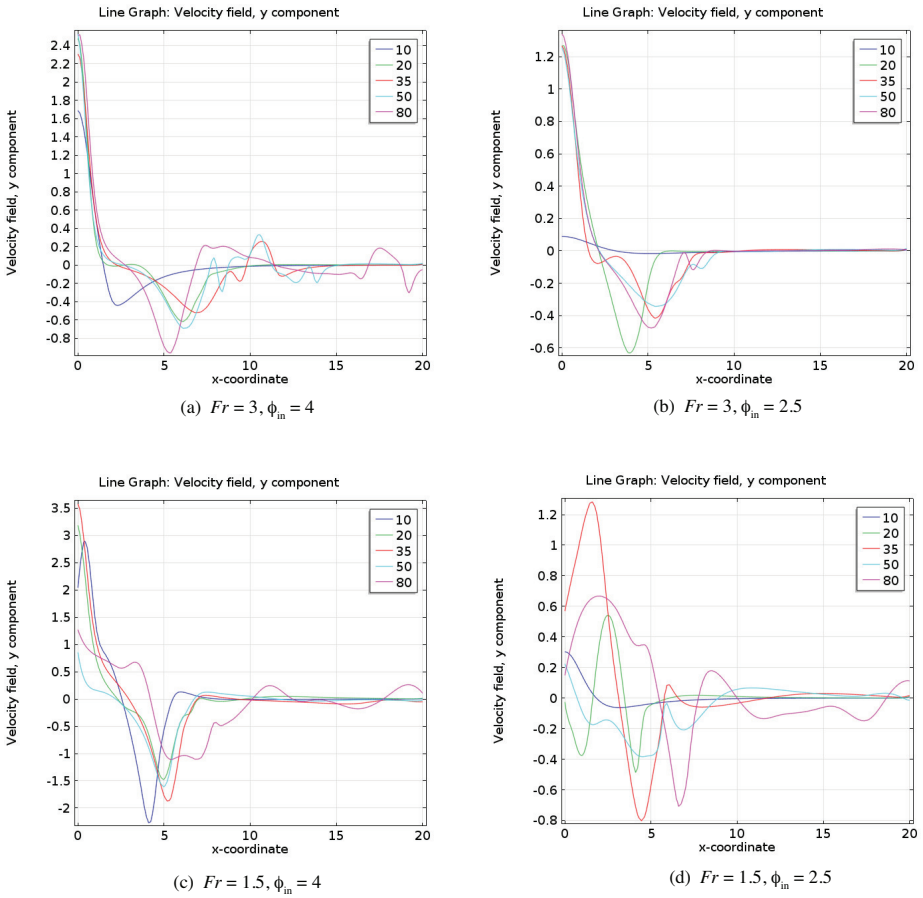

(a) $Fr = 3, \phi_{in} = 4$ (b) $Fr = 3, \phi_{in} = 2.5$

(c) $Fr = 1.5, \phi_{in} = 4$ (d) $Fr = 1.5, \phi_{in} = 2.5$

Figure 9: Horizontal profiles of vertical velocity component V at $Y = 9$ (near the ceiling), at times $\tau = 10, 20, 35, 50, 80$, for plumes with $Re = 50$, $Pr = 7$, and with Froude number and inlet temperature as indicated below each panel.

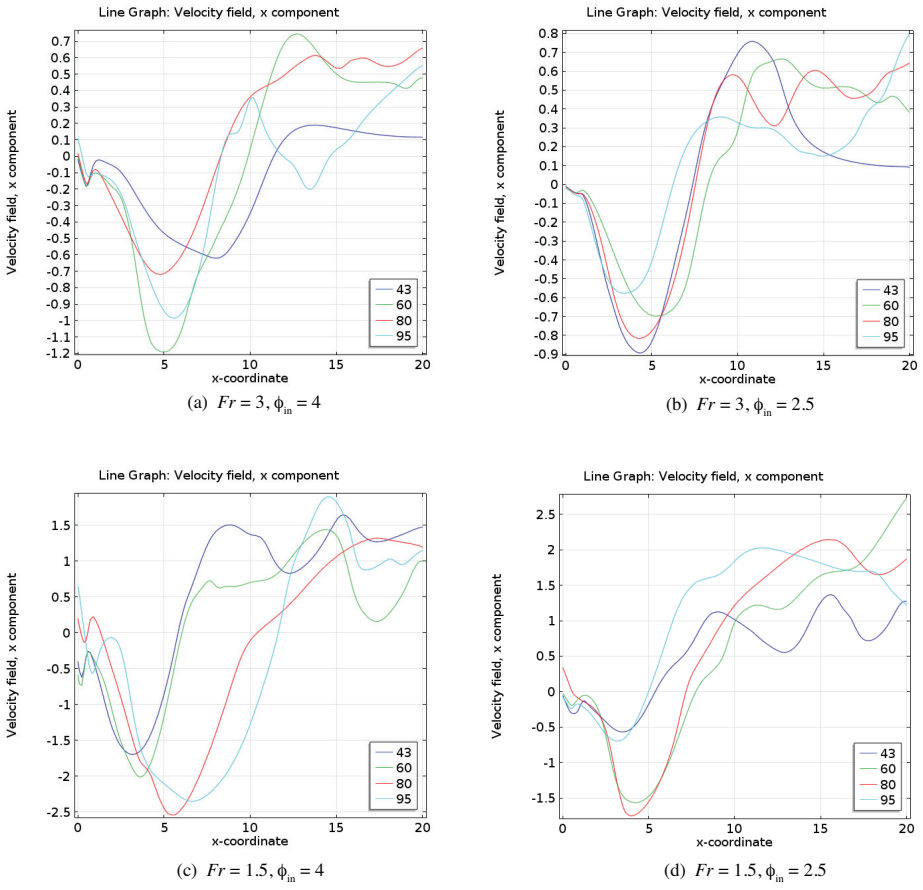

(a) $Fr = 3, \phi_{in} = 4$ (b) $Fr = 3, \phi_{in} = 2.5$

(c) $Fr = 1.5, \phi_{in} = 4$ (d) $Fr = 1.5, \phi_{in} = 2.5$

Figure 10: Horizontal profiles of horizontal velocity component U at $Y = 1$ (near the floor), at times $\tau = 43, 60, 80, 95$, for plumes with $Re = 50$, $Pr = 7$, and with Froude number and inlet temperature as indicated below each panel.

with a sloping flow descending to the floor on the outer side of the vortices; part of this is re-entrained into the central plume while the remainder of this dense, mixed fluid flows outward along the floor.

For small Froude numbers (exemplified in this study by computations with $Fr = 1.5$), the plume impinges rather weakly on the ceiling and then flaps from side to side, similarly to an unconfined plume. Similar flows were seen in [18] when the domain height was large; we have not varied the domain height, but we have used lower Froude numbers than in [18]. Large domain height can be considered as a proxy for small Froude number, because the height of (unconfined) plumes and fountains increases with Froude number.

The most interesting flows in the present study, which have no counterpart in the case of negatively buoyant fountains, are those found with $\phi_{\text{in}} = 4$ and $Fr \geq 2.5$. The initial development is similar to that with $\phi_{\text{in}} = 2.5$: the flow impinges on the ceiling, spreads some distance horizontally and then descends on the outer side of the vortices which were generated on either side of the central rising plume. This descent is reinforced by the presence of dense fluid resulting from mixing with the ambient. However, eventually a sufficient volume of unmixed, positively buoyant water emerges into the ceiling flow to separate from the descending flow, and after a "waiting period" this forms a gravity current along the ceiling. At the same time, dense mixed fluid in the descending flow forms a gravity current along the floor. A similar coexistence of light and dense gravity currents in cold water is observed in the experiments of Bukreev [6]. Ultimately, Bukreev's upper surface current is halted as it loses its buoyancy through mixing, but our simulations have not continued to that stage.

Due to the complexity of the flows described above, we have not attempted to determine any scalings of spreading distance as a function of either Froude number or inlet temperature. A further parameter of importance is Reynolds number; Srinarayana *et al.* found chaotic behaviour for $Re \geq 125$, but we have not varied our Reynolds number above 50. Our simulations at low Reynolds number could be validated by small-scale laboratory experiments; but for relevance to industrial discharges of warm water into cold lakes, for which the

Reynolds number would be many orders of magnitude greater, we will require simulations incorporating a turbulence model.

Acknowledgements

AMG gratefully acknowledges the funding for his PhD studies (of which this work forms part) provided by Niger Delta University, Bayelsa State, Nigeria.

References

[1] T.D. Foster, An analysis of the cabbeling instability in sea water. J. Phys. Oceanogr. 2 (1972) 294-301.

[2] J. F. Macqueen, Turbulence and cooling water discharges from power stations, in: C. J. Harris (Ed.), Mathematical Modelling of Turbulent Diffusion in the Environment, Academic Press, London, 1979, pp. 379-437.

[3] Y. R. Marmoush, A.A. Smith, P.F. Hamblin, Pilot experiments on thermal bar in lock exchange flow, Journal of Energy Engineering 110 (1984) 215-227.

[4] B. Hoglund, S.A. Spigarelli, Studies of the sinking plume phenomenon, in: Proceedings of the 15th Conference on Great Lakes Research, International Association of Great Lakes Research, Ann Arbor, MI, 1972, pp. 614-624.

[5] V.I. Bukreev, Effect of the nonmonotonic temperature dependence of water density on the decay of an initial density discontinuity, Journal of Applied Mechanics and Technical Physics 47 (2006) 54-60.

[6] V.I. Bukreev, Effect of the nonmonotonic temperature dependence of water density on the propagation of a vertical plane jet, Journal of Applied Mechanics and Technical Physics 47 (2006) 169-174.

[7] V.I. Bukreev, Plunging current caused by nonmonotonous water density dependence on temperature, Oceanology 51 (2011) 612-620.

[8] V.I. Bukreev, Effect of an anomalous temperature dependence of the water density on circular jet propagation, Fluid Dynamics 40 (2005) 202-208.

[9] V.I. Bukreev, A.V. Gusev, The effect of densification during mixing on the spreading of a vertical round jet, Doklady Earth Sciences 439 (2011) 1002-1005.

[10] A.M. George, A. Kay, Warm discharges in cold fresh water: 2. Numerical simulation of laminar line plumes, Environmental Fluid Mechanics (in press) DOI 10.1007/s10652-016-9468-x (2016).

[11] E.E. Zukoski, Fluid dynamic aspects of room fires, in: C.E. Grant, P.J. Pagni (Eds.), Fire Safety Science: Proceedings of the First International Symposium, Hemisphere Publishing Corporation, 1986, pp. 1-30.

[12] W.D. Baines, J.S. Turner, Turbulent buoyant convection from a source in a confined region, Journal of Fluids Mechanics 37 (1969) 51-80.

[13] N.B. Kaye, Y. Ji, M.J. Cook, Numerical simulation of transient flow development in a naturally ventilated room, Building and Environment 44 (2009) 889-897.

[14] T. Hattori, S.W. Armfield, M.P Kirkpatrick, Transitional ventilated filling box flow with a line heat source, International Journal of Heat and Mass Transfer 55 (2012) 3650-3665.

[15] M.D. Holstein, J.C. Lemckert, Spreading of energetic submerged fountains impinging on a rigid surface, in: Proceedings of the 14th Australasian Fluid Mechanics Conference, 2001, pp. 749-752.

[16] J. C. Lemckert, Spreading radius of fountains after impinging on a free surface, in: Proceedings of the 15th Australasian Fluid Mechanics Conference, 2004, pp. 217-220.

[17] P. Cooper, R.G. Hunt, Impinging axisymmetric turbulent fountains, Physics of Fluids 19 (2007) 117101.

[18] N. Srinarayana, W.S. Armfield, W. Lin, Impinging plane fountains in a homogeneous fluid, International Journal of Heat and Mass Transfer 52 (2009) 2614-2623.

[19] N. Srinarayana, W.S. Armfield, W. Lin, Laminar plane fountains impinging on a ceiling with an opposing heat flux, International Journal of Heat and Mass Transfer 52 (2009) 4545-4552.

[20] K.J. Ansong, J.P. Kyba, R.B. Sutherland, Fountains impinging on a density interface, J. Fluid Mech. 595 (2008) 115-139.

[21] D.R. Moore, N.O. Weiss, Nonlinear penetrative convection, J. Fluid Mech. 61 (1973) 553-581.

[22] P.H. Oosthuizen, J.T. Paul, A numerical study of the steady state freezing of water in an open rectangular cavity, Int. J. Numer. Meth. Heat Fluid Flow 6 (1996) 3-16.

[23] COMSOL Multiphysics Cyclopedia. The Finite Element Method (FEM), [ONLINE] Available at: https://www.comsol.com/multiphysics/finite-element-method, [Accessed 28 April 2016].